THE JOURNAL OF BIOLOGICAL CHEMISTRY Vol. 279, No. 41, Issue of October 8, pp. 42907–42915, 2004

Printed in U.S.A.

Structural Insights into the Catalytic Mechanism of Phosphate Ester Hydrolysis by dUTPase*+

Received for publication, June 2, 2004, and in revised form, June 15, 2004
Published, JBC Papers in Press, June 17, 2004, DOI 10.1074/jbc.M406135200

Orsolya Barabás‡§, Veronika Pongrácz‡, Júlia Kovári‡, Matthias Wilmanns¶, and Beáta G. Vértessy‡‖

From the ‡Institute of Enzymology, Biological Research Center, Hungarian Academy of Science, Budapest, Karolina út 29-31, H-1113, Hungary, the §Department of Theoretical Chemistry, Eötvös Loránd University, Budapest, H-1117 Hungary, and the ¶European Molecular Biology Laboratory, Hamburg Outstation, Hamburg, D-22603, Germany

dUTPase is essential to keep uracil out of DNA. Crystal structures of substrate (dUTP and *a*,*B*-imino-dUTP) and product complexes of wild type and mutant dUTPases were determined to reveal how an enzyme responsible for DNA integrity functions. A kinetic analysis of wild type and mutant dUTPases was performed to obtain relevant mechanistic information in solution. Substrate hydrolysis is shown to be initiated via in-line nucleophile attack of a water molecule oriented by an activating conserved aspartate residue. Substrate binding in a catalytically competent conformation is achieved by (i) multiple interactions of the triphosphate moiety with catalysis-assisting Mg^{2+}, (ii) a concerted motion of residues from three conserved enzyme motifs as compared with the apoenzyme, and (iii) an intricate hydrogen-bonding network that includes several water molecules in the active site. Results provide an understanding for the catalytic role of conserved residues in dUTPases.

This article was selected as a Paper of the Week by the Editor.

Papers of the Week:

dUTP Cleavage Clarified

J. Biol. Chem. 2004, 279:e99915.

Papers of the Week

dUTP Cleavage Clarified ♦

Because of its chemically reactive nature, the mammalian genome experiences numerous mutagenic and carcinogenic modifications on a daily basis. Fortunately, there are enzymes, such as dUTPase, whose sole duty is to preserve the integrity of DNA. dUTPase prevents the incorporation of uracil into DNA by catalyzing the cleavage of dUTP into dUMP and pyrophosphate. However, up until now the exact means by which dUTPase cleaved dUTP was a mystery. Although many crystal structures of dUTPase had been solved, no structure was able to provide an understanding of the enzyme's catalytic mechanism.

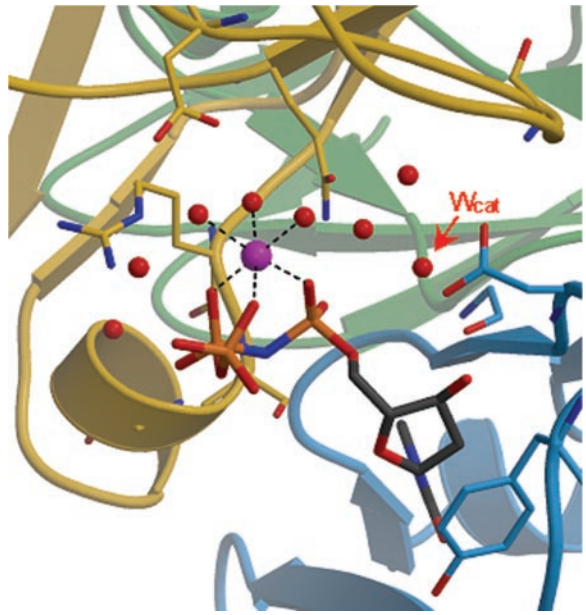

Locations of Mg^{2+} (*purple*) and catalytic water (*red*) in the dUTPase active site.

Orsolya Barabás and colleagues tackled this problem by doing three things: 1) the researchers replaced dUTP with the less reactive but similar interacting substrate analogue α,β-imino-dUTP; 2) they included the catalytic co-factor Mg^{2+} during complex formation; and 3) they used site-directed mutagenesis to replace the strictly conserved Asp^{90}, which is thought to activate a water molecule for nucleophilic attack, with asparagine. By comparing the crystal structures of these variations on dUTPase, Barabás *et al*. confirmed that substrate hydrolysis is initiated via in-line nucleophile attack of a water molecule oriented by Asp^{90}. The investigators also determined that catalytic substrate binding is achieved by multiple interactions between the triphosphate moiety and Mg^{2+}, as well as by a hydrogen-bonding network that includes several waters in the active site.

♦ See referenced article, *J. Biol. Chem. 2004,* **279,** 42907–42915

THE JOURNAL OF BIOLOGICAL CHEMISTRY
Vol. 279, No. 41, Issue of October 8, pp. 42907–42915, 2004

Printed in U.S.A.

Structural Insights into the Catalytic Mechanism of Phosphate Ester Hydrolysis by dUTPase*♦

Received for publication, June 2, 2004, and in revised form, June 15, 2004
Published, JBC Papers in Press, June 17, 2004, DOI 10.1074/jbc.M406135200

Orsolya Barabás‡§, Veronika Pongrácz‡, Júlia Kovári‡, Matthias Wilmanns¶, and Beáta G. Vértessy‡‖

From the ‡Institute of Enzymology, Biological Research Center, Hungarian Academy of Science, Budapest, Karolina út 29-31, H-1113, Hungary, the §Department of Theoretical Chemistry, Eötvös Loránd University, Budapest, H-1117 Hungary, and the ¶European Molecular Biology Laboratory, Hamburg Outstation, Hamburg, D-22603, Germany

dUTPase is essential to keep uracil out of DNA. Crystal structures of substrate (dUTP and α,β-imino-dUTP) and product complexes of wild type and mutant dUTPases were determined to reveal how an enzyme responsible for DNA integrity functions. A kinetic analysis of wild type and mutant dUTPases was performed to obtain relevant mechanistic information in solution. Substrate hydrolysis is shown to be initiated via in-line nucleophile attack of a water molecule oriented by an activating conserved aspartate residue. Substrate binding in a catalytically competent conformation is achieved by (i) multiple interactions of the triphosphate moiety with catalysis-assisting Mg^{2+}, (ii) a concerted motion of residues from three conserved enzyme motifs as compared with the apoenzyme, and (iii) an intricate hydrogen-bonding network that includes several water molecules in the active site. Results provide an understanding for the catalytic role of conserved residues in dUTPases.

Due to the chemical reactivity of DNA, numerous mutagenic and carcinogenic modifications to mammalian genome occur daily (1). Preserving DNA integrity is of vital importance. The ubiquitous enzyme dUTPase performs a key role in preventing uracil incorporation into DNA by catalyzing the cleavage of dUTP into dUMP and pyrophosphate (2). This reaction contributes to thymidylate biosynthesis and strictly controls cellular dUTP/dTTP ratios (3).

Targeting enzymes of *de novo* thymidylate biosynthesis by fluorouracil or methotrexate is a widely used approach in anticancer chemotherapy (4). These drugs perturb the cellular dUTP/dTTP pool resulting in synthesis of highly uracil-substituted DNA. Uracil-DNA transforms base-excision repair into a hyperactive cycle inducing DNA double-strand breaks and thymine-less cell death. This pathway preferentially kills cells actively synthesizing DNA, such as tumor and virus-infected cells. Moreover, in human cancer cell lines, dUTPase overexpression leads to development of fluorouracil resistance (5). Therefore, the clinical benefits of an anticancer therapy based on inducing thymine-less cell death may ultimately depend on the critical interplay among several enzymes involved in thymidylate metabolism. The recent finding of activation of dUTPase gene expression in p53 mutant tumor cells has reinforced the notion that this enzyme plays a significant role in tumor development and survival (6). The potential initiative role of dUTPase antagonism in thymine-less cell death has prompted investigations into the enzymatic mechanism.

Detailed description of the catalytic mechanism is central to enzymology (7–9). Although several dUTPase crystal structures at atomic to moderate resolution have already been published (10–14), mechanistic issues remain obscure. Using water labeled with ^{18}O, it was established that the water oxygen gets bonded to dUMP and not to the pyrophosphate, arguing for initiation of the reaction by nucleophilic attack at the α-phosphorus (15). A strictly conserved aspartate residue (Asp^{90} in the *Escherichia coli* enzyme) in a conserved sequence motif of dUTPases was suggested to activate a water molecule for the nucleophile attack (12, 13, 15). However, since the presumed catalytic water molecule could not be identified in the structures available to date, there are no reliable structural data about protein side chains involved in the hydrolytic reaction. Moreover, the possibility of a protein atom executing the initial nucleophilic attack could not have been excluded. The binding site of the Mg^{2+} co-factor was also not localized in the previously reported structures preventing structural insights into its functional role. Recently, the presence of Mg^{2+} was shown to facilitate substrate binding to both *E. coli* (16) and *Drosophila* dUTPases (17) (K_m decreases by ~0.5–1 order of magnitude) and to increase the value of k_{cat} 2–3-fold.

In the present work, we addressed the unresolved mechanistic issues by three-dimensional structural investigations and kinetic/mutagenesis studies. We determined crystal structures of the wild type *E. coli* dUTPase:α,β-imino-dUTP:Mg^{2+}, wild type dUTPase:dUMP, Asp^{90} → Asn mutant dUTPase:dUTP:Mg^{2+} and Asp^{90} → Asn mutant dUTPase:α,β-imino-dUTP:Mg^{2+} complexes (at 1.9-, 1.6-, 1.95-, and 1.7-Å resolution) complexes to identify conformational changes of protein side chains and their interactions with the ligand. A kinetic analysis was performed for the reaction of α,β-imino-dUTP hydrolysis by wild type dUTPase, as well as for the reaction of dUTP hydrolysis by Asp^{90} → Asn mutant dUTPase. Stepwise comparisons among these structures and the apoenzyme structure (11) together with the kinetic results revealed essential interactions required for catalysis and allowed novel insights into the mechanism.

* This work was supported by grants from the Hungarian National Research Foundation (T 034120, TS 044730, and M 27852 (to B. G. V.)); Howard Hughes Medical Institute Grant 55000342 (to B. G. V.); the Alexander von Humboldt Foundation, Germany; the Aventis/Institut de France Scientia Europeae Prize, France (to B. G. V.); and by the European Community-Improving the Human Research Potential and Socio-Economic Knowledge Base Programme-Marie Curie Training Sites, Contract HPMT-CT-20000-00174 (training to O. B.). The costs of publication of this article were defrayed in part by the payment of page charges. This article must therefore be hereby marked "*advertisement*" in accordance with 18 U.S.C. Section 1734 solely to indicate this fact.

♦ This article was selected as a Paper of the Week.

The atomic coordinates and structure factors (codes 1RN8, 1RNJ, 1SYL, and 1SHE) have been deposited in the Protein Data Bank, Research Collaboratory for Structural Bioinformatics, Rutgers University, New Brunswick, NJ (http://www.rcsb.org/).

‖ To whom correspondence should be addressed. E-mail: vertessy@enzim.hu.

EXPERIMENTAL PROCEDURES

Chemicals, Enzyme Preparation, and Purification—α,β-Imino-dUDP was obtained from Jena Bioscience. α,β-Imino-dUTP was prepared by enzymatic phosphorylation of α,β-imino-dUDP (18) and was shown to be over 98% pure by ion exchange chromatography (Fig. 1*A*). Other chemicals were of proanalysis quality from either Merck or Sigma.

The $Asp^{90} \rightarrow Asn$ mutant *E. coli* enzyme was created by QuikChange (Strategene) with mutagenic primers 5′-cctggtaggattgatcAACtctgactatcagggccag-3′ and 5′-ctggccctgatagtcagaGTTgatcaatcctaccagg-3′ on plasmid pET3a-dut (19). Wild type and $Asp^{90} \rightarrow Asn$ mutant *E. coli* dUTPase was expressed and purified as described previously (16). Enzyme kinetic parameters toward dUTP were measured by the continuous spectrophotometric assay as described in Refs. 17 and 20. α,β-Imino-dUTP hydrolysis was followed in reaction mixtures of 3 mg/ml *E. coli* dUTPase and 1–10 mM α,β-imino-dUTP in 0.1 M Tris buffer, pH 7.8, 5 mM $MgCl_2$, also containing 400 mM sodium acetate, at room temperature. The decrease of α,β-imino-dUTP levels and production of dUMP was followed in aliquots taken at different time points to be analyzed either on a Mono Q anion exchange column or by thin layer chromatography (17).

Protein Crystallization and Data Collection—Crystals were obtained at 20 °C by hanging-drop vapor diffusion. The protein/ligand solution prepared for co-crystallization contained 3 mg/ml enzyme, 1.25 mM α,β-imino-dUTP, or 5 mM dUTP, or 1.25 mM dUMP, and 10 mM $MgCl_2$ in 10 mM Tris/HCl buffer, pH 7.0, and 50 mM NaCl. dUTPase:ligand:Mg^{2+} solution was mixed with equal volume of reservoir solution (0.1 M Tris/HCl buffer, pH 7.8, containing 18–20% polyethylene glycol 3350 and 400 mM sodium acetate). For data collection, crystals were introduced into cryoprotectant containing 10% glycerol and appropriate amounts of ligand in reservoir solution, then flash-frozen in a 100 K nitrogen stream. Three data sets were collected at various synchrotron beamlines at European Molecular Biology Laboratory/German Electron Synchrotron Facility (DESY) (Hamburg, Germany): wild type *E. coli* dUTPase:α,β-imino-dUTP:Mg^{2+} at PX11, wild type *E. coli* dUTPase:dUMP:Mg^{2+} at PX13, and mutant *E. coli* dUTPase:dUTP:Mg^{2+} at BW7B; while the fourth data set of the mutant *E. coli* dUTPase:α,β-imino-dUTP:Mg^{2+} was collected at the ID14-4 European Synchrotron Radiation Facility (Grenoble, France). Data processing and scaling were carried out using MOSFLM (21) and SCALA (22) or XDS (23).

Catalytic competence of the enzyme in the crystal phase was checked by competition experiments with the native substrate dUTP. Crystals of wild type dUTPase containing α,β-imino-dUTP were washed with reservoire solution and dUTP was added at 10 mM concentration. Hydrolysis was followed by discontinuous thin layer chromatography activity test (24).

Structure Determination and Refinement—Structures of wild type and $Asp^{90} \rightarrow Asn$ mutant dUTPases, in complexes with α,β-imino-dUTP:Mg^{2+}, dUTP:Mg^{2+}, and dUMP, were solved by molecular replacement (MOLREP (25)). The apo-dUTPase structure (11) was used as search model for all the four presently determined structures to exclude any model bias with respect to the ligand position. The asymmetric unit contained one monomer. In each case, the resultant initial maps were of exceptional quality, allowing residues 1–136 and entire ligands to be built with ease.

Generation of monomer libraries for the ligands (α,β-imino-dUTP, dUTP) and refinement were carried out using CCP4i and Refmac5 (22). Positional and *B*-factor refinement rounds were altered with manual rebuilding steps using the graphics program O (26), and ARP/wARP (27) was used for water building. Residues belonging to the C-terminal Motif V (residues 137–152) are hardly visible even in the final maps and are therefore mostly omitted from the model. A summary of the crystallographic data collection and refinement statistics is given in Table II.

Coordinates and structure factor data have been deposited in the Protein Data Bank with accession codes 1RN8, 1RNJ, 1SYL, and 1SEH, for the wild-type enzyme-α,β-imino-dUTP complex, the $Asp^{90} \rightarrow Asn$ enzyme-α,β-imino-dUTP complex, the $Asp^{90} \rightarrow Asn$ enzyme-dUTP complex, and the wild type enzyme-dUMP complex, respectively.

The figures were produced using Molscript v2.1.2 (28), Raster3D v2.7b (29), and Bobscript v2.6b (30).

Simulated annealed omit electron density maps (sigma-weighted $2F_o - F_c$ maps) were calculated using CNS v1.1, omitting the entity in question and a 3.5-Å region surrounding it. The figures are restricted to show only the entity in question.

RESULTS

The Experimental Approach—Previous dUTPase complex structures identified the protein fold and the overall characteristics of active site architecture; however, they failed to provide an understanding of the catalytic mechanism (10, 12–14). This failure was probably due to the fact that these structures represented dead-end enzyme-inhibitor complexes. To produce the relevant enzyme-substrate complexes with lifetimes allowing crystallographic characterization, we considered the following potentials.

First, the substrate dUTP was replaced by the substrate analogue α,β-imino-dUTP. Imino analogues of nucleotide phosphates are commonly used as isosteric mimics of the natural substrates (31, 32) both with respect to bond distances (1.63 and 1.68 Å, for P–O–P and P–N–P moieties, respectively) and bond angles (128.7° and 127.2°, for P–O–P and P–N–P, respectively) (33). The lower electronegativity of the nitrogen atom results in less reactivity of the phosphate ester imino analogues. Nevertheless, several enzymes (*e.g.* small GTPase p21 (34), sarcoplasmic reticulum ATPase (35), and alkaline phosphatase (36)) were reported to catalyze imino-linkage cleavage, arguing for some reactivity associated with the P–N–P moiety. Fig. 1*A* demonstrates that dUTPase is also capable of hydrolyzing the imino-linkage of α,β-imino-dUTP, while no detectable hydrolysis of the β-γ bond occurs, *i.e.* the exclusive specificity of dUTPases for α-β bond cleavage is retained in the reaction with the imino analogue as well. Table I summarizes kinetic and ligand binding data for the dUTPase-catalyzed dUTP and α,β-imino-dUTP hydrolysis. The very low k_{cat} value in the α,β-imino-dUTP hydrolysis reaction rendered K_m determination unreliable; therefore the previously determined K_d value is presented for comparison (37). Assuming rapid equilibrium reactions, as suggested by an earlier kinetic analysis (15), K_m and K_d values are expected to be the same. The very close agreement in the nucleotide interaction data (K_m, K_d, *cf.* Table I) for dUTP and the analogue α,β-imino-dUTP strongly suggests highly similar accommodation patterns for these two hydrolysable nucleotides in the dUTPase active site, although the rate of hydrolysis differs by almost 6 orders of magnitude. Based on these kinetic and ligand binding data, both the enzyme-dUTP and the enzyme-α,β-imino-dUTP complex will be termed in the present work as enzyme-substrate complexes (Fig. 1*B*).

Second, the dUTPase catalytic co-factor Mg^{2+} ion (15, 16), not yet localized in any previously reported crystal structure (10–14, 38, 39), was also included during complex formation. Mg^{2+} binding in the enzyme:α,β-imino-dUTP/dUTP complexes was promoted by novel crystallization conditions at neutral or slightly basic pH values, since deprotonation of side chains has a well known positive effect on metal ion coordination capability. Earlier crystallization solvents contained either acidic buffers (11, 12, 38) or high concentrations of metal-chelating citrate (13, 39).

Third, a site-directed mutation was designed to exchange the strictly conserved aspartate side chain (Asp^{90}) within the active site into an asparagine residue. This mutation was expected to decrease the reaction rate and allow for a structural analysis of the enzyme-dUTP complex in the presence of the co-factor Mg^{2+} ion.

Structure of Enzyme-Substrate Complex—dUTPases show exquisite substrate specificity with respect to base, sugar, and phosphate chain moieties of dUTP that is essential to prevent unintended hydrolysis of other high energy-containing nucleotides. Most dUTPases are homotrimers (Fig. 2*A*) with five conserved sequence motifs in each monomer (Fig. 2*B*) (10, 12–14). Consensus sequences for conserved dUTPase motifs

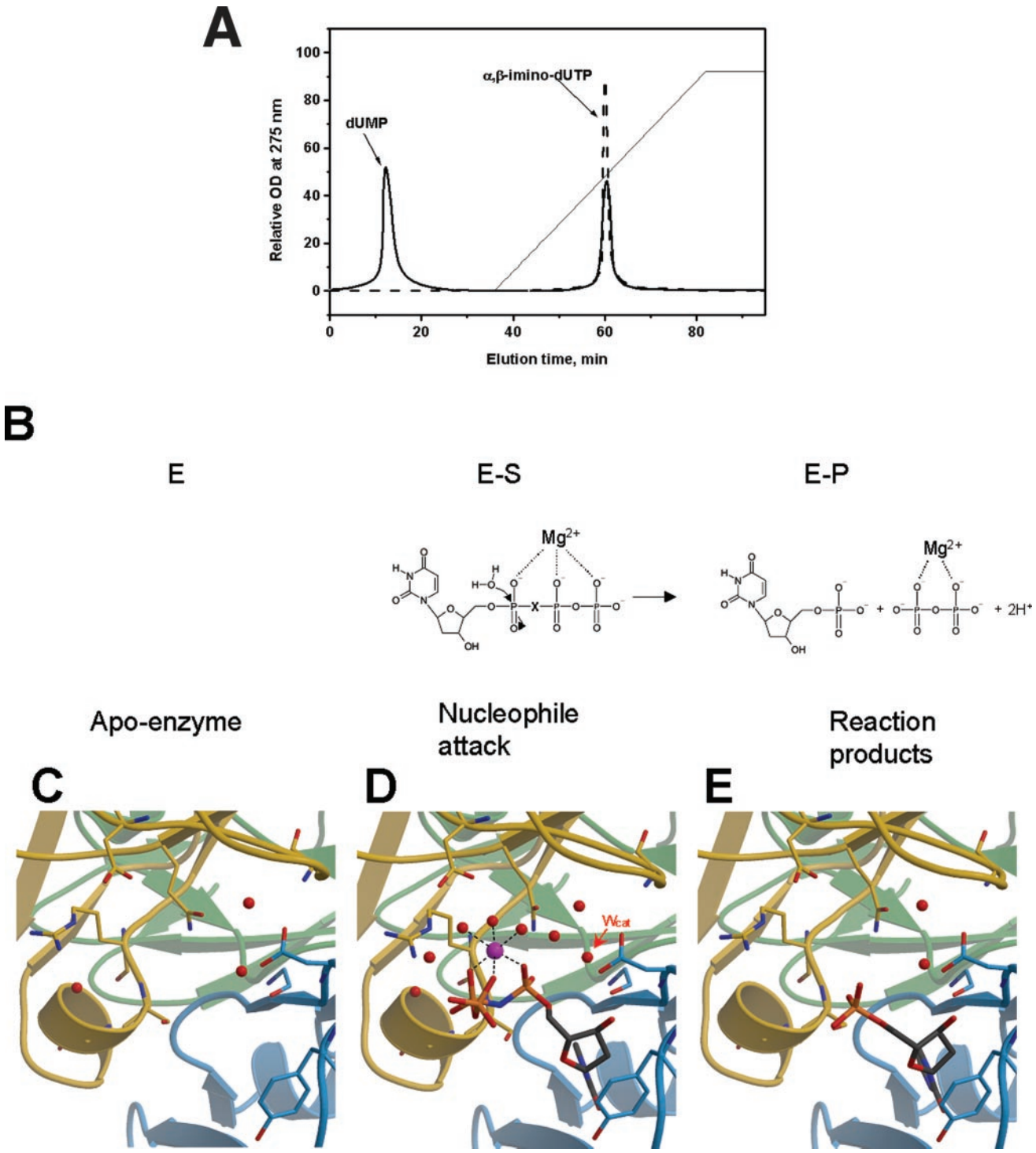

FIG. 1. **Reactions catalyzed by dUTPase.** *A*, experimental observation of α,β-imino-dUTP hydrolysis. Reaction mixtures (*cf.* "Experimental Procedures") were set up in the absence (*thick dashed trace*) or in the presence (*thick solid trace*) of *E. coli* dUTPase and were incubated for 2 weeks at room temperature. Chromatograms represent the nucleotide composition; *arrows* indicate the corresponding elution positions of dUMP and α,β-imino-dUTP standards. The *thin line* represents the salt gradient applied in the chromatography. *B*, theoretical reaction schemes of dUTP (*X* = O) or α,β-imino-dUTP (*X* = N) hydrolysis. The catalytic water molecule initiating nucleophile attack and the Mg^{2+} ion coordinated to the triphosphate chain are shown as determined in the crystal structure (*D*). In the reaction products, the Mg^{2+}-pyrophosphate interaction is hypothetic, the hypothesis being based upon the apparent absence of the Mg^{2+} from the dUTPase:dUMP structure. *C*, *D*, and *E*, active-site close-ups of apoenzyme, dUTPase:α,β-imino-dUTP:Mg^{2+}, and dUTPase:dUMP structures, respectively. In the subunit-color-coded ribbon model of the protein, the side chain and/or main chain atoms of some conserved residues (Tyr^{93}, Asp^{90}, Leu^{88} from monomer A, Ala^{29}, Asp^{32}, Arg^{71}, Ser^{72}, Gly^{73}, and Gln^{119} from monomer B) important in active site architecture are also shown, together with some significant water molecules. For denominations of these residues and waters, omitted from this figure to avoid small print details, please refer to Fig. 3*A* that presents the active site in the same orientation. The ligands and the non-carbon protein atoms are in atom coloring bonds model (carbon, *dark gray*; oxygen, *red*; phosphorus, *orange*; nitrogen, *blue*; magnesium, *purple*). The apoenzyme structure was taken from the literature (11).

are: Motif I, Ala-Gly-(Pho)-Asp-Leu; Motif II, (Pro/Gly)-(Arg/Lys)-Ser; Motif III, Gly-$(Pho)_2$-Asp-$(Nnn)_2$-Tyr-(Nnn)-Gly; Motif IV, Arg-(Pho)-Ala-Gln; Motif V, Arg-Gly-$(Nnn)_2$-Gly-Phe-Gly-(Ser/His)-(Thr/Ser)-Gly (amino acids in three-letter codes: Pho, hydrophobic residue; Nnn, any residue) (10, 40). Overall fold and active site architecture are notably well conserved

TABLE I

Kinetic and ligand binding data for wild type and Asp^{90} → Asn mutant E. coli dUTPase

Data represent the average of three to five independent measurements. Standard error of k_{cat} and K_m determination was 12 and 17%, respectively. ND, not determined.

Nucleotide	Wild type			Asp^{90} → Asn mutant		
	k_{cat}	K_m	k_{cat}/K_m	k_{cat}	K_m	k_{cat}/K_m
	s^{-1}	μM	$M^{-1}\ s^{-1}$	s^{-1}	μM	$M^{-1}\ s^{-1}$
dUTP	11	0.5	1.4×10^7	2.55×10^{-4}	0.45	850
α,β-Imino-dUTP	2×10^{-5}	1.0[a]	20[b]	ND	ND	ND

[a] K_d from Ref. 37.
[b] k_{cat}/K_d.

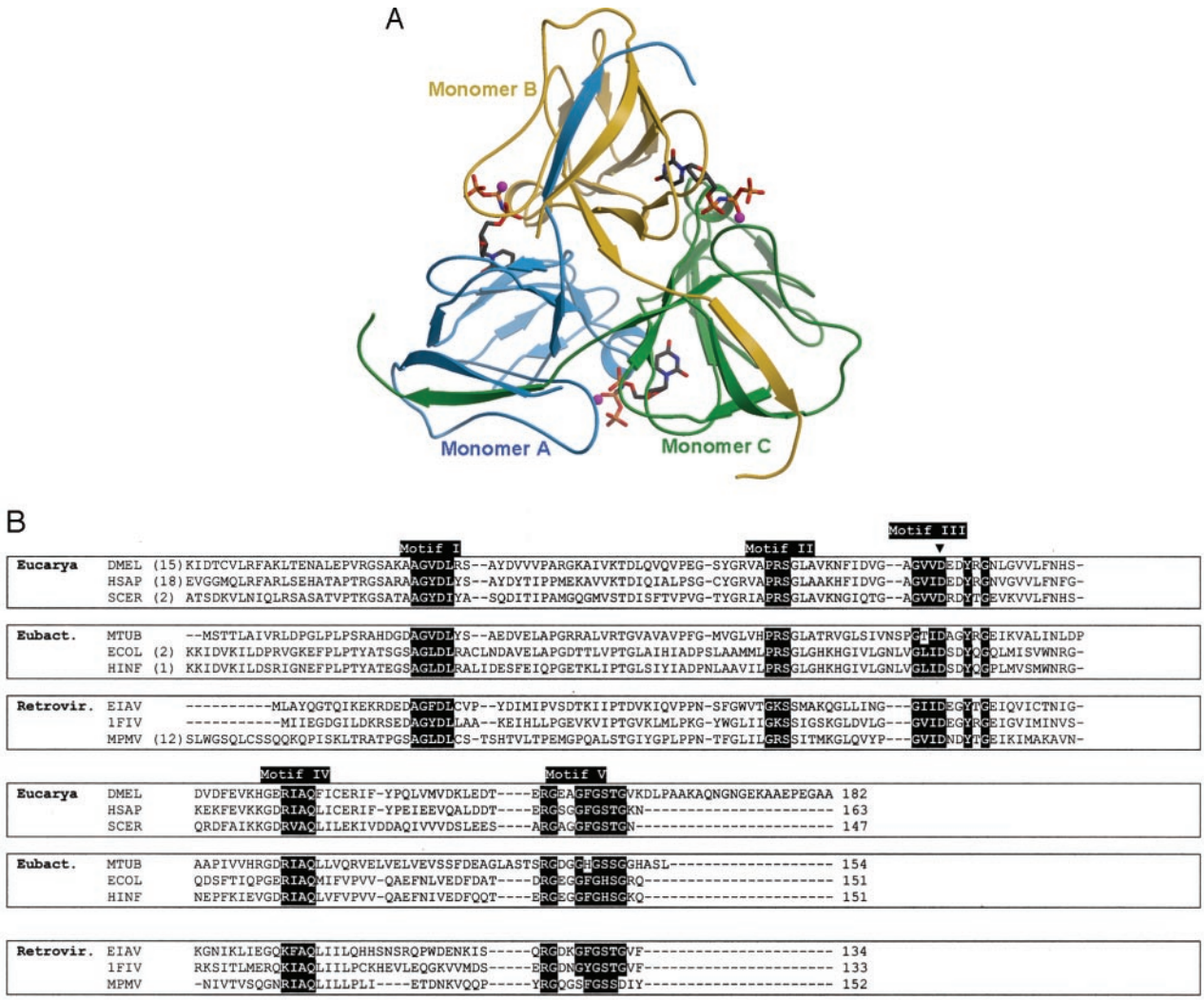

FIG. 2. *A*, overall structure of dUTPase. Enzyme-substrate (E. coli dUTPase:α,β-imino-dUTP:Mg^{2+}) complex. The trimer is shown with ribbon model of color-coded (code retained throughout the present study, where applicable) subunits and bonds model of the nucleotide ligand molecule in the three active sites. Mg^{2+}-ions are represented as purple balls. *B*, Sequence alignments of dUTPases. Conserved residues within the five (I-V) dUTPase motifs are in bold white on black background. Arrowhead points at the conserved aspartate in Motif III, Asp90 in the *E. coli* sequence, which was selected for the Asn mutation.

among dUTPases from retroviruses and bacteria to man (10, 12–14).

To study the first step of the reaction, the structure of the dUTPase:α,β-imino-dUTP:Mg^{2+} complex (Figs. 1*D*, 2*A*, 3, *A*, *B*, *D*, *E*, and 4*A* and Table II) was determined at 1.9-Å resolution. In agreement with previous studies (10, 12–14), each β-pleated subunit forms jellyroll topology and contributes the C-terminal β-strand to the neighboring subunit. The three active sites of the homotrimer are located in clefts between neighboring monomers and recruit conserved motifs from different subunits in a 3-fold symmetric pattern (Fig. 2*A*). A β-hairpin formed by conserved Motif III from monomer A accommodates the uracil and sugar rings. A conserved tyrosine (Tyr^{93}) stacks to the 2′-deoxyribose ring and sterically excludes ribonucleotides. Phosphate chain recognition is provided by conserved Motifs I, II, and IV of monomer B (Figs. 1, *D* and *E*, and 3). Therefore, active site architecture ultimately depends on correct oligomerization of the homotrimer. To our present knowledge, this organization of ligand binding sites is unique among proteins.

The present structure localizes the catalysis-assisting physiological co-factor Mg^{2+}, not seen in any previously reported structure, and the entire triphosphate chain of the hydrolyz-

TABLE II
Crystallographic data collection and refinement statistics
WT indicates wild type enzyme. Values in parentheses correspond to the highest resolution shell.

	WT-dUTPase:α,β-imino-dUTP:Mg^{2+}	D90N mutant dUTPase:α,β-imino-dUTP:Mg^{2+}	D90N mutant dUTPase:dUTP:Mg^{2+}	WT-dUTPase:dUMP
Space group	$P6_322$	$P6_322$	$P6_322$	$P6_322$
Cell parameters *a*, *c* (Å)	74.6, 99.6	74.9, 99.6	75.3, 98.8	75.3, 100.5
Data collection				
Wavelength (Å)	0.8110	0.9392	0.8414	0.8040
Resolution (Å)	27.1–1.9 (1.98–1.93)	22.0–1.7 (1.74–1.70)	20.0–1.91 (2.03–1.91)	20.0–1.5 (1.60–1.47)
Measured reflections	128,620 (6,183)	372,822 (26,388)	38,679 (6,077)	930,805 (129,002)
Unique reflections	12,804 (819)	18,346 (1,268)	13,413 (2,085)	29,251 (6,421)
Completeness (%)	99.2 (99.2)	98.2 (98.2)	98.3 (98.5)	99.9 (100.0)
$I/\sigma(I)$	10.3 (2.8)	8.4 (2.0)	15.0 (2.5)	27.6 (4.9)
R_{sym} (%)[a]	6.1 (26.8)	5.9 (38.0)	6.3 (48.4)	8.3 (73.0)
Refinement statistics				
Resolution (Å)	20.0–1.93	20.0–1.70	20.0–1.95	20.0–1.47
Nonhydrogen atoms	1317	1353	1250	1298
Water molecules	191	221	167	194
Data:parameter:restraint	12,892:5,278:16,976	18,811:5,422:17,195	13,200:5,010:16,328	29,279:5,202:16,906
r.m.s. deviation bonds (Å)[b]	0.016	0.019	0.020	0.021
r.m.s. deviatoin angles (°)[b]	1.60	1.54	1.69	1.38
R_{work} (%)[c]	13.7	15.7	15.8	15.8
R_{free} (%)[c,d]	18.0	18.7	18.9	18.4

[a] $R_{sym} = \Sigma\,\Sigma_j|I_j - \langle I\rangle|/\Sigma\langle I\rangle$, where I_j is the recorded intensity of the *j*th reflection and $\langle I\rangle$ is the average intensity over multiple recordings.
[b] Root mean square deviation from ideal/target geometries.
[c] $R_{work,\ free} = \Sigma||F_{obs}| - |F_{calc}||/|F_{obs}|$.
[d] R_{free} values are calculated for a randomly selected 5% of the data that was excluded from the refinement.

able substrate α,β-imino-dUTP in the enzyme active site with low crystallographic *B*-factors, indicating a well ordered assembly (*cf.* Table II, first data column). Detailed analysis of the catalytically competent enzyme conformation provides novel determinant features of the enzymatic mechanism. All three phosphate groups are within the coordination sphere of the well defined metal ion that also receives coordination through water molecules coordinated by Asp^{32} and Gln^{119} of subunit B (Figs. 3*A* and 4*A*). The α-phosphate oxygens are contacted by Nϵ2 of the same Gln^{119}, and the main chain NH of Ser^{72} from subunit B, while Arg^{71} of subunit B reaches toward the β- and γ-phosphates (Figs. 3*A* and 4*A*). Some water molecules are well localized (with temperature factors 17, 8, 18, 14, and 12 $Å^2$, for W1, W2, W4, W15, and W21, respectively, to be compared with the average temperature factor of 17.4 $Å^2$) around the phosphate oxygens. These waters play a crucial role in mediating interactions between the protein residues and the phosphate oxygens.

Comparison of apoenzyme and enzyme-substrate complex shows only minor conformational shifts in the active site, and most of these are involved in residues of subunit B, responsible for phosphate accommodation. The movement of Arg^{116} and Arg^{71} by 1.23 and 0.88 Å, respectively, provide phosphate chain interactions, while Gln^{119} adopts an altered conformation for proper hydrogen-bonding geometry. The catalytic site in the apoenzyme already presents side chain conformations adequate for binding of the uracil and deoxyribose moieties, alleviating the need for significant changes induced by the incoming dUTP (Figs. 1, *C* and *D*, and 3*D*).

Identification of the Nucleophile Responsible for Attack at the α-Phosphorus—The present dUTPase-substrate complex structure allows identification of the attacking nucleophile. A search along the axis of the α-phosphorus-imino nitrogen bond located a single possible candidate for in-line nucleophile attack: a water oxygen (termed W_{cat}, numbered as W5 in the 1RN8 coordinate file, *red arrow* in Figs. 1*D* and 3, *A* and *B*, *cf.* also Fig 4A) coordinated to Asp^{90} in monomer A (previously suggested to be a catalytic residue (12)). No other protein or water atoms were found within 4.0 Å to the α-phosphorus, emphasizing the special role of the proximal water (W_{cat}). A simulated annealed omit map, calculated with omission of entities in the 3.5 Å radius region around this water, was created for its clear localization (Fig. 3*A*). Both carboxyl oxygens of Asp^{90} may participate in hydrogen-bonding to W_{cat}. AspOδ2 is also within H-bonding distance to the deoxyribose 3′-OH group, while AspOδ1 is H-bonded to monomer B Ala^{29} main chain NH and another water (W4) that contacts monomer B Gln119 through W1 (Figs. 3*A* and 4*A*). The monomer B Ala^{29} main chain H-bond may play a role in orienting the Asp^{90} side chain. No other side chain atoms were closer than 4.0 Å to this putative catalytic water. However, another protein atom (Leu88 main chain carbonyl O) is also within H-bonding distance to W_{cat} as discussed below. This arrangement suggested that replacing only one side chain oxygen of Asp^{90} with an amino group might drastically affect enzyme function. The $Asp^{90} \rightarrow$ Asn mutant was constructed and proved to be largely compromised in catalytic efficiency (Table I). k_{cat}/K_m for the mutant was determined to be 850 $M^{-1}\,s^{-1}$ as compared with 3.5×10^7 $M^{-1}\,s^{-1}$ for wild type, a decrease of almost 5 orders of magnitude. Importantly, K_m was the same for both mutant and wild type enzymes (0.45 *versus* 0.5 μM) (Table I), indicating that substrate accommodation is the same in both species. The crystal structure of the $Asp^{90} \rightarrow$ Asn mutant in complex with Mg^{2+} and α,β-imino-dUTP was solved at 1.7-Å resolution and is shown as superimposed on the wild type complex structure (Fig. 3*B*, *cf.* also Fig 3F, and Table II). The superimposed structures are practically indistinguishable (r.m.s.[1] for fitting of all atoms is 0.12), except for the catalytic water electron density (Fig. 3, *A*, *B*, *E*, and *F*) that is missing from the mutant complex structure. A straightforward interpretation of this result is that replacing AspOδ2 with an NH_2 group with altered H-bonding characteristics adversely interferes with W_{cat} coordination in the $Asp^{90} \rightarrow$ Asn mutant. A rotation of AsnOδ1 (the corresponding atom for AspOδ1) into the AspOδ2 position could theoretically provide proper coordination for W_{cat}, but this rotation is impeded by the AsnOδ1-monomer B Ala^{29} main chain H-bond, also present with AspOδ1 in the wild type complex.

[1] The abbreviation used is: r.m.s., root mean square.

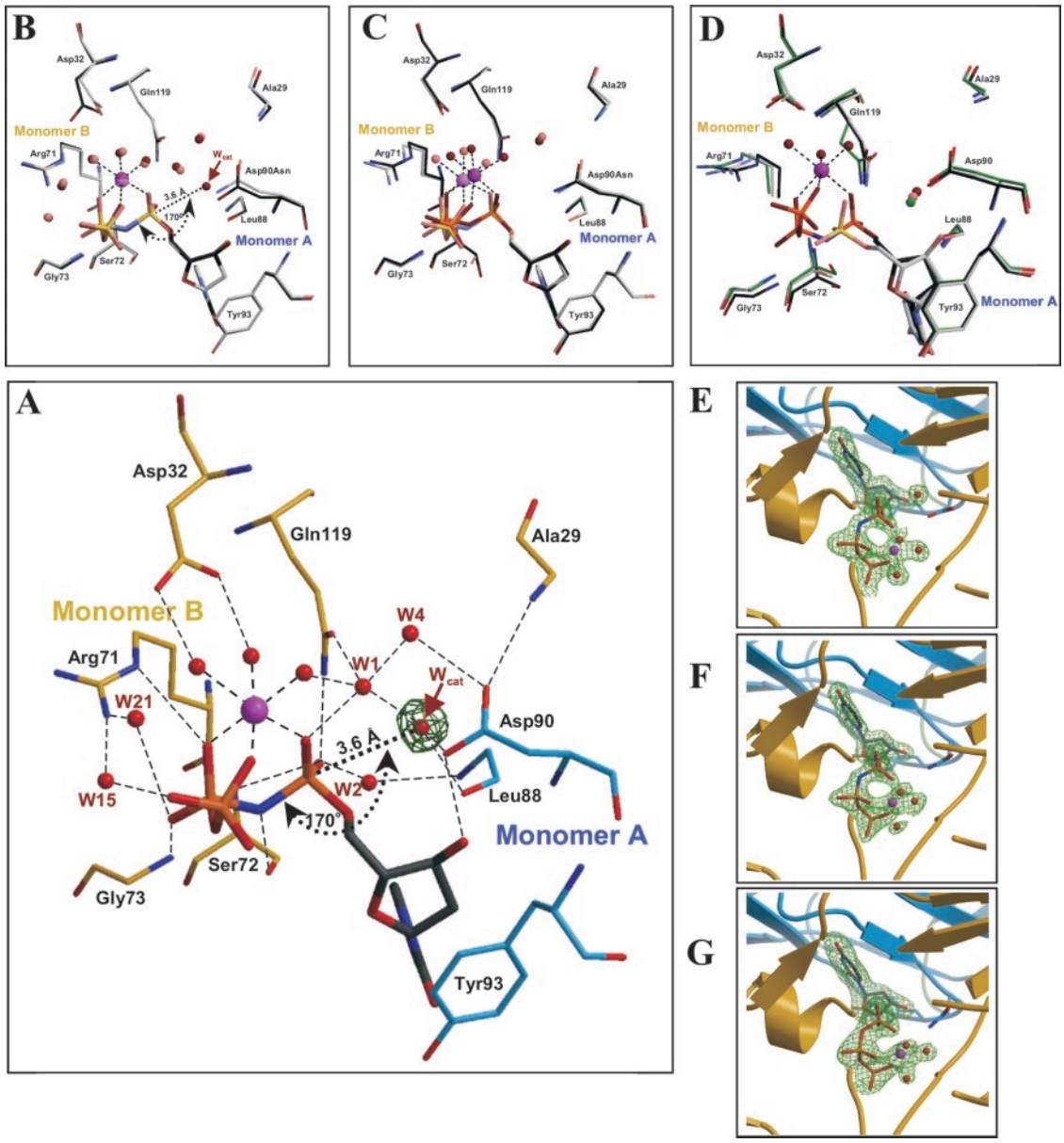

FIG. 3. **Identification of the nucleophile water.** *A*, simulated annealed omit electron density map, restricted to exclusively show the exact position of the catalytic water molecule in the wild type dUTPase:α,β-imino-dUTP:Mg^{2+} structure. The figure also shows the hydrogen-bonding network involving the phosphate chain in this complex structure. In addition to the catalytic water, Mg^{2+}-coordinating waters, W1, W2, W4, W15, and W21, also participate in the primary hydrogen-bonding interactions. *B*, superimposed structures of wild type (*dark tones*) and $Asp^{90} \rightarrow Asn$ mutant (*light tones*) dUTPase:α,β-imino-dUTP:Mg^{2+} complexes. Note that the only remarkable difference between the superimposed structures is the disappearance of W_{cat} from the mutant complex. Atomic color code: carbon, *dark/light gray*; oxygen, *dark/light red* (*pink*); phosphorus, *dark/light orange* (*yellow*); nitrogen, *dark/light blue*; magnesium, *dark/light purple*. *C*, superimposed structures of $Asp^{90} \rightarrow Asn$ mutant dUTPase:dUTP:Mg^{2+} (*dark tones*) and $Asp^{90} \rightarrow Asn$ mutant dUTPase:α,β-imino-dUTP:Mg^{2+} (*light tones*) complexes. Note the close identity in the positions of the nucleotide ligands. *D*, apoenzyme retains a water closely corresponding to the W_{cat} position. 3-Fold superimposition of the apoenzyme (*green* carbons and water, otherwise standard atom coloring), enzyme-substrate (*dark tones*), and enzyme-product (*light tones*) structures. Note the position of the catalytic water from the apoenzyme to the enzyme-substrate and enzyme-product complexes. *E*, *F*, and *G*, simulated annealed omit electron density maps for the substrates in wild type *E. coli* dUTPase:α,β-imino-dUTP:Mg^{2+}, the $Asp^{90} \rightarrow Asn$ *E. coli* dUTPase:α,β-imino-dUTP:Mg^{2+}, and the $Asp^{90} \rightarrow Asn$ *E. coli* dUTPase:dUTP:Mg^{2+} structures, respectively. Maps are restricted to show the nucleotide ligand, the Mg^{2+}, the three water molecules coordinating to the metal ion, as well as the catalytic water, if present.

The very low enzymatic activity of the $Asp^{90} \rightarrow Asn$ mutant rendered it possible to determine the crystal structure of the mutant enzyme:dUTP:Mg^{2+} complex (Figs. 3, *C* and *G*, Table II). In this structure, substrate and Mg^{2+} accommodation patterns are highly similar to those realized in the enzyme:α,β-imino-dUTP:Mg^{2+} complex (Fig. 3, *C*, *F*, and *G*). All atoms of the imino analogue and the physiological substrate, including the α-phosphate group where nucleophilic attack occurs, are well superimposable (r.m.s. is 0.179).

These structures, together with the kinetic data, clearly demonstrate that the water molecule termed W_{cat} provides the attacking nucleophile oxygen. Although the structures that identified W_{cat} have been determined for the α,β-imino-dUTP complexes of wild type and $Asp^{90} \rightarrow Asn$ mutant dUTPases, the catalytic incompetence of the $Asp^{90} \rightarrow Asn$ mutant was proved in the physiological reaction (dUTP hydrolysis). Therefore, the Asp^{90} residue plays a determinant role in dUTP hydrolysis, too. Two roles have been associated with this residue: (i) coordination of deoxyribose 3′OH (Figs. 3*A* and 4*A*, *cf.* also Refs. 10, 12–14) and (ii) H-bonding to W_{cat} (Figs. 3*A* and 4*A*). The $Asp^{90} \rightarrow Asn$ (*i.e.* $Asp^{90}O\delta2 \rightarrow Asn^{90}N\delta2$) mutant is not compromised in the first role (*cf.* equal accommodation of dUTP as

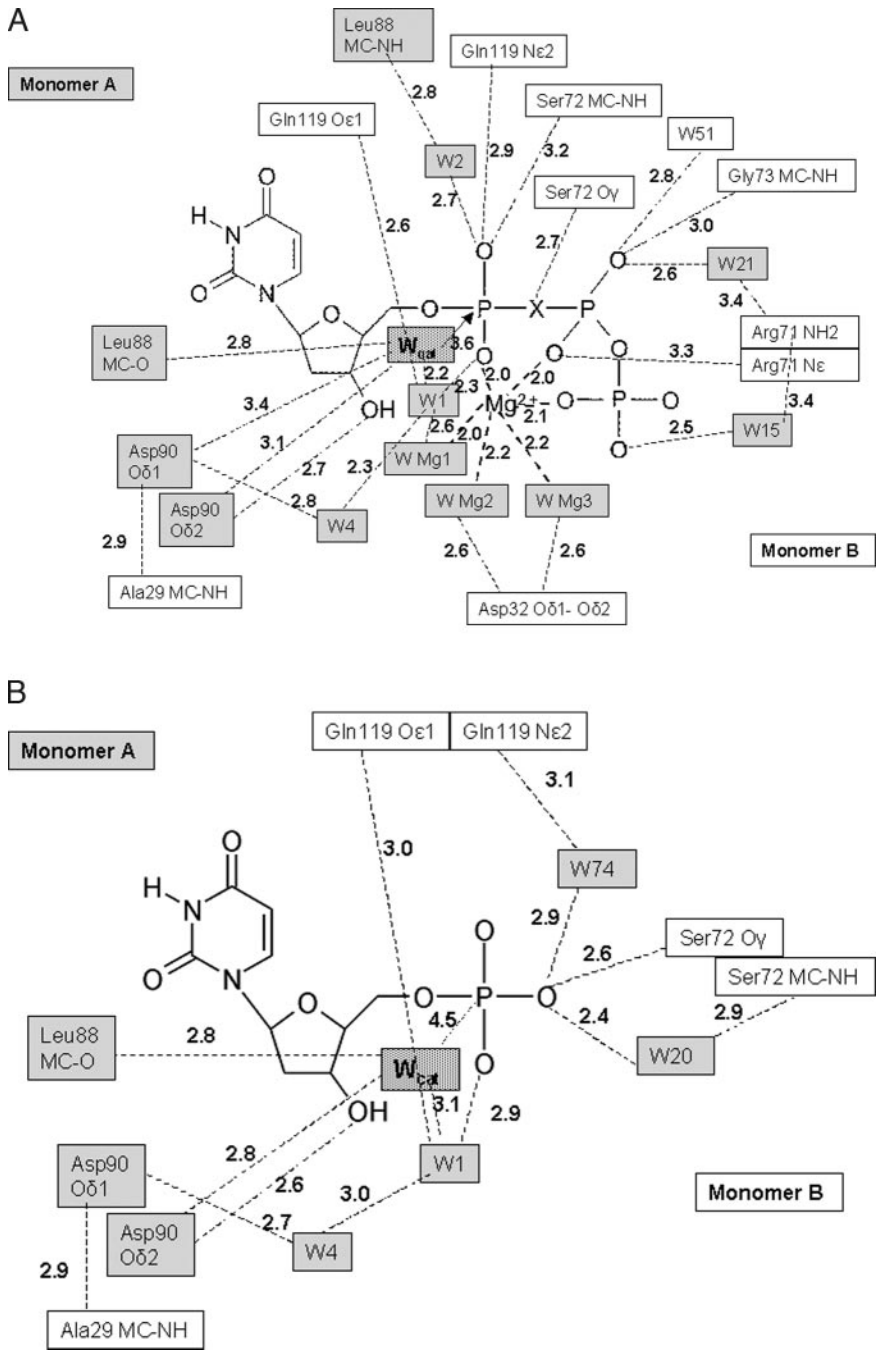

FIG. 4. **Interaction mapping in enzyme-substrate (*A*), and enzyme-product complexes (*B*).** Interactions are shown only for the phosphate chain moiety of the ligand. Due to the close similarity of the nucleotide interactions in the three enzyme-substrate complexes determined in the present study (*cf.* Fig. 3 and Table I), the map was selected to show the actual distances as found in the wild type dUTPase:α,β-imino-dUTP:Mg^{2+} (X = N) complex where W_{cat} is also present. In the $Asp^{90} \rightarrow$ Asn mutant dUTPase:α,β-imino-dUTP:Mg^{2+} (X = N) and Asp90 $\rightarrow$ Asn mutant dUTPase:dUTP:Mg^{2+} (X = O) complex, the only significant differences are that (i) W_{cat} is absent and $Asp^{90}O\delta2$ becomes $AsnN\delta2$ and (ii) in the $Asp^{90} \rightarrow$ Asn mutant dUTPase:dUTP:Mg^{2+} (X = O) complex, the X-$Ser^{72}O\gamma$ interaction is absent. Changes in all other distances are within ±0.2 Å.

evidenced by K_m values in Table I and three-dimensional structures in Fig. 3, *B*, *E*, and *F*). Consequently the attenuated catalytic efficiency of the mutant enzyme is most probably due to lack of proper coordination to the catalytic water molecule in the physiological reaction. In addition, phosphate chain conformations in the dUTPase:α,β-imino-dUTP:Mg^{2+} and dUTPase:dUTP:Mg^{2+} complexes are identical (Fig. 3*C*), indicating that the nucleophile attack mechanism should be similar in both cases.

Interestingly, the catalytic water molecule seems to be present in the apoenzyme structure (1EUW (11)), as well (W334 at a distance of 0.86 Å to the W_{cat} position, *cf.* also Fig 3*D*). It is coordinated to $Asp^{90}O\delta2$, as well as to the Leu^{88} main chain carbonyl oxygen, just as it is found in the presently determined enzyme:α,β-imino-dUTP:Mg^{2+} complex (Fig. 3*D*). In the latter complex, W_{cat} clearly adopts a closely co-linear location to the scissile bond to carry out nucleophilic attack on the α-phosphate. In the enzyme-product complex structure, as detailed below (Table II, Figs. 1*E*, 3*D*, and 4*B*), the W_{cat} proximal water (W49) has again the same coordination pattern. In summary, W_{cat} (or the W_{cat} proximal water) coordinates to the same protein atom ligands ($Asp^{90}O\delta2$ and Leu^{88} main chain O) in all these structures. We propose that these two protein ligands, with the possible participation of other water molecules, create a binding site for W_{cat} that is, in fact, one of the substrates required for the dUTP hydrolysis reaction (dUTP + H_2O = dUMP + PP_i, *cf.* Fig 1*B*). This binding site is already available in the absence of the nucleotide substrate. After completion of the catalytic reaction, products (dUMP and PP_i) are expected to be exchanged for substrates (dUTP and H_2O). Following the two-substrate analogy, the presence of W_{cat} in the enzyme-product complex may be interpreted as recruitment of a solvent water molecule in such an exchange reaction.

Completion of the Catalytic Cycle—The pyrophosphate group

at the entrance of the active site is expected to exit freely as it can easily make numerous contacts with the bulk solvent. The metal ion may facilitate pyrophosphate discharge since it is more likely to bind to the pyrophosphate (charge minus 4) as compared with dUMP (charge minus 2 at physiological pH). Accordingly, no electron density could be assigned to Mg^{2+} in the enzyme-product structure, although the dUTPase-dUMP complex has been crystallized in the presence of the metal ion (Table II and Figs. 3*D* and 4*B*). The C-terminal Motif V from monomer C, mostly disordered in our present and also in previously reported structures, may also participate in pyrophosphate escape via charge stabilization with its strictly conserved Arg^{141} side chain. Preferential discharge of the pyrophosphate moiety over the dUMP is also strengthened by x-ray crystallographic investigations carried out on dUTPase crystals soaked into substrate containing solution that retained dUMP, but not the pyrophosphate moiety, in the enzyme active site (14).

Figs. 3*D* and 4, *A* and *B*, indicate that the reaction product dUMP retains most of the binding interactions found with the substrate with respect to the sugar and base moieties. However, some side chains providing interactions with the triphosphate moiety (*e.g.* monomer B side chains Asp^{32}, Arg^{71}, Ser^{72}, and Gln^{119}) are shifted back to their positions occupied in the apoenzyme (Fig. 3*D*). This shift may contribute to the significant decrease of dUMP binding affinity to dUTPase, when compared with dUDP, dUTP, and α,β-imino-dUTP (15, 37). Less tight binding of dUMP as compared with dUTP facilitates exchange of product with substrate in the active site whenever substrate is available in the bulk phase.

DISCUSSION

The side-by-side three-dimensional structural analysis of the apoenzyme, as well as substrate, and product complexes delineated atomic interactions crucial to the catalytic mechanism of dUTPase. The conclusions were based on structures and kinetic data determined with the imino substrate analogue, as well as the physiological substrate and the physiological product. Several results indicate that the reaction pathway may well be of similar character with both dUTP and α,β-imino-dUTP. First, a water molecule in the immediate vicinity to the presently determined W_{cat} is localized already in the apoenzyme structure and is also present in the enzyme-dUMP complex (Fig. 3*D*). Second, the binding position of the physiological substrate dUTP, most importantly the entire phosphate chain conformation, is equivalent to that of the imino analogue (Fig. 3. *C*, *F*, and *G*). Third, the $Asp^{90} \rightarrow Asn$ mutation was shown to adversely affect W_{cat} coordination and, parallel to this, to inactivate the enzyme in the physiological reaction. It is therefore reasonable to assume that (i) a water molecule coordinated to Asp^{90} and Leu^{88} is present with high probability in the active site of the wild type enzyme when dUTP is also bound, and (ii) this water molecule is poised for in-line attack, well within 4.0 Å to the α-phosphorus. Given such an arrangement, it can be assumed that this specific water will act as the nucleophile in dUTP hydrolysis.

The Metal Ion Site—The localization of the site for the catalysis-assisting Mg^{2+} provided significant novel insights, as well. Its important role in providing catalytically competent accommodation of the substrate in the dUTPase active site, as judged by k_{cat} and K_m determinations in the presence and absence of the metal ion, was well established in a number of earlier studies on dUTPases from diverse sources (15–17, 24). It was also well known that divalent metal ions usually contribute to enzymatic reactions of nucleotides by coordinating the otherwise quite flexible phosphate chain. Consequently, absence of the active site Mg^{2+} from the earlier determined crystal structures prevented the definition of the catalytically competent phosphate chain conformation, thereby rendering the identification of the nucleophile attacker impossible. The data on the dUTPase:dUDP:Sr^{2+} complex were a significant step forward in this problem (10). However, due to the diminished catalytic competence of the Sr^{2+} substitution as well as the altered coordination geometry of the Sr^{2+} (coordination number 8) as compared with Mg^{2+} (coordination number 6), the character of the nucleophile attack could not be determined before. In fact, in the dUTPase:dUDP:Sr^{2+} complex, the critical position of the α-phosphorus is 3.2 Å away from its competent site as determined in our present dUTPase:dUTP:Mg^{2+} and Mg^{2+}:α,β-imino-dUTP:dUTPase structures. The coordination of Mg^{2+} to all the three phosphate groups is not very common in other nucleotide-protein structures where the metal ion is frequently seen as coordinating to only two phosphate groups (41–44). In the dUTPase structures, the triple phosphate coordination of Mg^{2+} contributes to an increasingly compact phosphate chain conformation presumably optimal for catalysis.

Role of Conserved Residues—The enzymatic reaction is facilitated by non-covalent bonding interactions and involves residues from different monomers, as well as several water molecules bound within the active sites. All residues proposed to interact with ligand and W_{cat} are strictly conserved among dUTPase sequences. The contacts and role of some of these residues, like those of the β-hairpin, Ile^{89}, Asp^{90}, Tyr^{93}, Ser^{72}, Arg^{71}, Arg^{116}, and Gln^{119}, were already suggested based on previously determined crystal structures of *E. coli*, equine infectious anemia virus (EIAV), feline immunodeficiency virus (FIV), and *Homo sapiens* dUTPases (10, 12–14). However, as previous studies failed to define a catalytically competent substrate conformation, the relevant roles of conserved residues need to be reinterpreted in the light of our present data.

In general, the conclusions drawn from our structures concerning the role of Gly^{73} main chain nitrogen and Arg^{71} guanidino group in coordination and charge distribution of the phosphate chain, especially the β- and γ-phosphates correspond well with suggestions supported by previously determined structures of dUTPases from various sources (10, 12–14). However, the interaction between the phosphate chain and Arg^{71} became water-mediated in our structures. This difference might be ascribed to the effective charge stabilization provided by the Mg^{2+} in our structures. Due to the presence of Mg^{2+}, the triphosphate chain adopts a more compact conformation that increases its distance from the Arg^{71} guanidino group. The weaker charge stabilization effect of the Arg^{71} side chain is probably compensated for by the Mg^{2+} ion.

The compact character of the phosphate chain in the present structures also shifts the interaction between the Ser^{72} main chain NH and an oxygen in the β-phosphate group to another oxygen in the α-phosphate group. This shift may contribute to activation of the α-phosphorus for the nucleophile attack and might stabilize the developing charge in the transition state.

The present data provide detailed characterization of role of Asp^{32} as well. In the previous retroviral dUTPase:dUDP:Sr^{2+} complex structure (10), one of the carboxyl oxygens of this conserved residue (Asp^{20} in the retroviral sequence) was within H-bonding distance to one of the eight coordinating ligands of the Sr^{2+} ion. The large size of Sr^{2+}, its altered coordination geometry, and poor catalytic competence, however, attenuated the relevance of the $Mg^{2+} \rightarrow Sr^{2+}$ substitution for mechanistic conclusions. In the present structures, both side chain oxygens of Asp^{32} take part in coordination of two water molecules in the coordination sphere of the physiological metal ion that has six ligands.

The Catalytic Water—We presented a description of the catalytic pathway via identification of the nucleophile agent and

characterization of interactions responsible for building up the required arrangement and initiating the reaction. The key residue here, Asp^{90}, was previously shown to contribute to substrate binding via H-bonding to the OH group of the ribose. A general base-like role was also suggested, but in the absence of the identification of the nucleophile attacker atom, this role could not have been clarified. In the present structures, one of the side chain oxygens of Asp^{90} (Oδ2) provides close coordination to the catalytic water, and Asp^{90}Oδ1 is also nearby (Fig. 4*A*). Importantly, the present structural data also show that the proper orientation of the critical Asp^{90} side chain is provided by an interaction between one of its other carboxyl oxygens (Oδ1) and the main chain NH of the conserved Ala^{29} from the neighboring subunit. This connection is strictly retained in all other dUTPase structures, as well, but no importance was ascribed to it. It also explains why the $Asp^{90} \rightarrow Asn$ mutant is so much attenuated in catalytic efficiency and ineffective in coordinating the W_{cat}. In the mutant, the Ala^{29} main chain NH retains its interaction with Oδ1 of the Asn^{90} residue, leaving only the nitrogen atom of the mutant (Nδ2) for the role of close coordination to the catalytic water molecule. The nitrogen atom, however, cannot fulfill this role efficiently.

We also identified a second protein atom ligand of W_{cat}. The main chain carbonyl oxygen of Leu^{88}, a conserved hydrophobic residue together with Asp^{90} creates a well defined binding site for this water that is the second substrate of the enzyme.

At last, significance of Gln^{119} (Motif IV) has also been discovered in this study. Its side chain oxygen (Oϵ1) coordinates a water molecule (W1) that provides H-bonding in the water network around W_{cat}. The Gln^{119} side chain amino group participates in H-bonding to one of the oxygens on the reaction center α-phosphorous.

The Character of Phosphate Ester Hydrolysis—Available data for non-enzymatic phosphate diester hydrolysis reactions are in favor of a mechanism with significant associative character, since the metaphosphate transition state required for the dissociative mechanism is highly unstable when an additional bulky ligand is present (45, 46). Our present results for the dUTPase-catalyzed reaction are in agreement with this expectation. In our structure, the distance between the entering oxygen and the phosphorus reaction center is 3.6 Å with an experimental error of 0.164 Å based on the Luzzati plot (47), while a minimum of 4.9 Å is considered to be required for the dissociative mechanism (*cf.* Ref. 48). The present data show co-linearity of W_{cat} with the scissile bond for in-line attack that can also be reconciled with a mechanism of significant associative character.

Acknowledgments—We gratefully thank Profs. Gábor Náray-Szabó and Richard I. Gumport for fruitful discussions. We also thank Dr. Alexander Popov and Katja Schirwitz for helpful suggestions in crystallization and x-ray diffraction, Imre Zagyva for excellent technical assistance, Rebecca Persson for the expression plasmid, and beamlines and operators at European Molecular Biology Laboratory/German Electron Synchrotron Facility (DESY) (Hamburg, Germany) and ID14-4 European Synchrotron Radiation Facility (Grenoble, France) for data collection opportunities.

REFERENCES

1. Friedberg, E., Walker, G., and Siede, W. (1995) *DNA Mutagenesis and Repair*, pp. 108–133, ASM Press, Washington, D. C.
2. Shlomai, J., and Kornberg, A. (1978) *J. Biol. Chem.* **253,** 3305–3312
3. Pearl, L. H., and Savva, R. (1996) *Nat. Struct. Biol.* **3,** 485–487
4. Aherne, G. W., and Browne, S. (1999) in *Anticancer Development Guide: Antifolate Drugs in Cancer Therapy* (Jackman, A. L., ed) pp. 409–421, Humana Press, Inc., Totowa, NJ
5. Canman, C. E., Radany, E. H., Parsels, L. A., Davis, M. A., Lawrence, T. S., and Maybaum, J. (1994) *Cancer Res.* **54,** 2296–2298
6. Pugacheva, E. N., Ivanov, A. V., Kravchenko, J. E., Kopnin, B. P., Levine, A. J., and Chumakov, P. M. (2002) *Oncogene* **21,** 4595–4600
7. Benkovic, S. J., and Hammes-Schiffer, S. (2003) *Science* **301,** 1196–1202
8. Knowles, J. R. (1991) *Nature* **350,** 121–124
9. Schowen, R. L. (1978) in *Transition States of Biochemical Processes* (Gandour, R. D., and Schowen, R. L., eds) pp. 77–113, Plenum Press, New York
10. Dauter, Z., Persson, R., Rosengren, A. M., Nyman, P. O., Wilson, K. S., and Cedergren-Zeppezauer, E. S. (1999) *J. Mol. Biol.* **285,** 655–673
11. Gonzalez, A., Larsson, G., Persson, R., and Cedergren-Zeppezauer, E. (2001) *Acta Crystallogr. D. Biol. Crystallogr.* **57,** 767–774
12. Larsson, G., Svensson, L. A., and Nyman, P. O. (1996) *Nat. Struct. Biol.* **3,** 532–538
13. Mol, C. D., Harris, J. M., McIntosh, E. M., and Tainer, J. A. (1996) *Structure* (*Lond.*) **4,** 1077–1092
14. Prasad, G. S., Stura, E. A., Elder, J. H., and Stout, C. D. (2000) *Acta Crystallogr. D. Biol. Crystallogr.* **56,** 1100–1109
15. Larsson, G., Nyman, P. O., and Kvassman, J. O. (1996) *J. Biol. Chem.* **271,** 24010–24016
16. Mustafi, D., Bekesi, A., Vertessy, B. G., and Makinen, M. W. (2003) *Proc. Natl. Acad. Sci. U. S. A.* **100,** 5670–5675
17. Kovari, J., Barabas, O., Takacs, E., Bekesi, A., Dubrovay, Z., Pongracz, V., Zagyva, I., Imre, T., Szabo, P., and Vertessy, B. G. (2004) *J. Biol. Chem.* **279,** 17932–17944
18. Persson, T., Larsson, G., and Nyman, P. O. (1996) *Bioorg. Med. Chem.* **4,** 553–556
19. Persson, R., Nord, J., Roth, R., and Nyman, P. O. (2002) *Prep. Biochem. Biotechnol.* **32,** 157–172
20. Vertessy, B. G. (1997) *Proteins* **28,** 568–579
21. Leslie, A. G. W. (1992) *Joint CCP4 & ESF-EAMCB Newslett. Protein Crystallogr.* **26,**
22. Collaborative Computational Project 4 (1994) *Acta Crystallogr. Sect. D. Biol. Crystallogr.* **50,** 760–763
23. Kabsch, W. (1993) *J. Appl. Crystallogr.* **26,** 795–800
24. Barabas, O., Rumlova, M., Erdei, A., Pongracz, V., Pichova, I., and Vertessy, B. G. (2003) *J. Biol. Chem.* **278,** 38803–38812
25. Vagin, A., and Teplyakov, A. (1997) *J. Appl. Crystallogr.* **30,** 1022–1025
26. Jones, T. A., Zou, J. Y., Cowan, S. W., and Kjeldgaard, M. (1991) *Acta Crystallogr. Sect. A* **47,** 110–119
27. Lamzin, V. S., and Wilson, K. S. (1993) *Acta Crystallogr. D. Biol. Crystallogr.* **49,** 129–149
28. Kraulis, P. J. (1991) *J. Appl. Crystallogr.* **24,** 946–950
29. Merritt, E. A., and Bacon, D. J. (1997) *Methods Enzymol.* **277,** 505–524
30. Esnouf, R. M. (1999) *Acta Crystallogr. D. Biol. Crystallogr.* **55,** 938–940
31. Hirshberg, M., Stockley, R. W., Dodson, G., and Webb, M. R. (1997) *Nat. Struct. Biol.* **4,** 147–152
32. Pai, E. F., Kabsch, W., Krengel, U., Holmes, K. C., John, J., and Wittinghofer, A. (1989) *Nature* **341,** 209–214
33. Larsen, M., Willett, R., and Yount, R. G. (1969) *Science* **166,** 1510–1511
34. Pai, E. F., Krengel, U., Petsko, G. A., Goody, R. S., Kabsch, W., and Wittinghofer, A. (1990) *EMBO J.* **9,** 2351–2359
35. Taylor, J. S. (1981) *J. Biol. Chem.* **256,** 9793–9795
36. Yount, R. G., Babcock, D., Ballantyne, W., and Ojala, D. (1971) *Biochemistry* **10,** 2484–2489
37. Vertessy, B. G., Larsson, G., Persson, T., Bergman, A. C., Persson, R., and Nyman, P. O. (1998) *FEBS Lett.* **421,** 83–88
38. Cedergren-Zeppezauer, E. S., Larsson, G., Nyman, P. O., Dauter, Z., and Wilson, K. S. (1992) *Nature* **355,** 740–743
39. Prasad, G. S., Stura, E. A., McRee, D. E., Laco, G. S., Hasselkus-Light, C., Elder, J. H., and Stout, C. D. (1996) *Protein Sci.* **5,** 2429–2437
40. Fiser, A., and Vertessy, B. G. (2000) *Biochem. Biophys. Res. Commun.* **279,** 534–542
41. Theis, K., Chen, P. J., Skorvaga, M., Van Houten, B., and Kisker, C. (1999) *EMBO J.* **18,** 6899–6907
42. Ostermann, N., Schlichting, I., Brundiers, R., Konrad, M., Reinstein, J., Veit, T., Goody, R. S., and Lavie, A. (2000) *Struct. Fold. Des.* **8,** 629–642
43. Ling, H., Boudsocq, F., Woodgate, R., and Yang, W. (2001) *Cell* **107,** 91–102
44. Flachner, B., Kovari, Z., Varga, A., Gugolya, Z., Vonderviszt, F., Naray-Szabo, G., and Vas, M. (2004) *Biochemistry* **43,** 3436–3449
45. Williams, N. H. (2004) *Biochim. Biophys. Acta* **1697,** 279–287
46. Wolfenden, R. (1998) *J. Am. Chem. Soc.* **120,** 833–834
47. Luzzati, V. (1952) *Acta Crystallogr.* **5,** 802–810
48. Mildvan, A. S. (1997) *Proteins* **29,** 401–416